A Recipe for the Computation of the Free Energy Barrier and the Lowest Free Energy Path of Concerted Reactions[†]

Bernd Ensing,*,‡ Alessandro Laio,§ Michele Parrinello,§ and Michael L. Klein‡

Center for Molecular Modeling and Department of Chemistry, University of Pennsylvania, 231 South 34th Street, Philadelphia, Pennsylvania 19104-6323, and Computational Science, Department of Chemistry and Applied Biosciences, ETH Zurich, USI Campus, Via Giuseppe Buffi 13, CH-6900 Lugano, Switzerland

The recently introduced hills method (*Proc. Natl. Acad. Sci. U.S.A.* **2002,** *99,* 12562) is a powerful tool to compute the multidimensional free energy surface of intrinsically concerted reactions. We have extended this method by focusing our attention on localizing the lowest free energy path that connects the stable reactant and product states. This path represents the most probable reaction mechanism, similar to the zero temperature intrinsic reaction coordinate, but also includes finite temperature effects. The transformation of the multidimensional problem to a one-dimensional reaction coordinate allows for accurate convergence of the free energy profile along the lowest free energy path using standard free energy methods. Here we apply the hills method, our lowest free energy path search algorithm, and umbrella sampling to the prototype S_N2 reaction. The hills method replaces the in many cases difficult problem of finding a good reaction coordinate with choosing relatively simple collective variables, such as the bond lengths of the broken and formed chemical bonds. The second part of the paper presents a guide to using the hills method, in which we test and fine-tune the method for optimal accuracy and efficiency using the umbrella sampling results as a reference.

I. Introduction

The intrinsic reaction coordinate (IRC)[1,2] is defined as the steepest descent path on the potential energy surface, in mass-weighted Cartesian coordinates, that connects the (chemical) reactant state with the product state. Given the transition state, the IRC is routinely computed,[3−5] and the evolution of a reacting system along this minimal energy reaction path may thus be followed. However, finding the transition state in the first place remains, in many cases, an art. Moreover, when temperature and entropy effects are important, the *free* energy surface has to be explored so that the transition state cannot be found with the canonical gradient methods nor is there a straightforward way to compute a lowest free energy reaction path. Resolving the reaction paths that lead through the rugged (free) energy landscape is an important but challenging step in understanding chemical reaction mechanisms. Much effort has been put into improving the conventional Newton−Raphson methods to find saddle points (transition states) by following the local curvature of the energy surface and to find reaction pathways from there.[6−9] Alternatively, a number of recent developments to find reaction paths are based on generating and optimizing alternative routes from an initial path that connects two stable states (reactants and products).[10−18]

Techniques to compute reaction free energy profiles, such as umbrella sampling and constrained molecular dynamics, depend heavily on an appropriate reaction coordinate—the lowest free energy path (or at least a good approximation to it) would be ideal.[19] In practice, one usually has to settle with a chemically intuitive internal coordinate, for example, a bond length or a torsion angle. Unfortunately, this approach often fails in delivering the desired reaction free energy profile since contributions from other internal coordinates are neglected with such a simple choice for the reaction coordinate. Examples are the reaction flux result for the NaCl dissociation in aqueous solution using the Na−Cl bond distance as the reaction coordinate[20] and the constrained molecular dynamics (MD) study of the S_N2 reaction between $Cl^−$ and CH_3Cl in aqueous solution with the reaction coordinate being a function only of the two C−Cl distances.[21] In both cases, the omission of the solvent degrees of freedom that describe the activated (de-)solvation of the ions along the reaction path leads to too low a transition state barrier. Collective variables that capture the relevant solvent degrees of freedom would be, for example, the coordination number[22] and the local electrostatic field.[23] However, adding several collective variables into a single one-dimensional reaction coordinate is usually not possible, as their functionality is not known a priori. Instead, the collective variables should be sampled independently. Unfortunately, the computational effort of constrained MD scales exponentially with the dimension, and for umbrella sampling finding a good one-dimensional biasing potential is usually already cumbersome, let alone finding a multidimensional one.

Recently Laio and Parrinello introduced a powerful method to efficiently compute multidimensional free energy surfaces as a function of a limited set of collective variables using coarse-grained non-Markovian MD.[24,25] The characteristic feature of this method, in some way related to the local elevation technique,[26] is the gradual buildup of a history-dependent biasing potential that discourages the system from revisiting points in configurational space. The biasing potential thus builds up rapidly in the local reactant and product wells, allowing the system to sample the important but unfavorable transition and intermediate states. The free energy profile is obtained from

---

Computations for Concerted Reactions

J. Phys. Chem. B, Vol. 109, No. 14, 2005 **6677**

the accumulated biasing potential to arbitrary accuracy using small enough Gaussian hills.

In the present work, we build on this (hills) method by localizing the lowest free energy reaction path connecting the reactant well with the product well in the reduced multidimensional free energy surface obtained with the hills method. The lowest free energy path (LFEP) is the important property that describes the most probable reaction mechanism, similar to the zero temperature IRC, but also includes finite temperature effects. We employ the LFEP as the reaction coordinate to perform, now one-dimensional, umbrella sampling, where we use the multidimensional free energy surface to obtain a good one-dimensional biasing umbrella potential. Recently, we reported in a brief communication on this approach applied to the elimination (E2) reaction between fluoroethane and a fluoride ion.[27] The main advantages of combining the hills method with umbrella sampling are that (1) the free energy profile converges usually even faster within one-dimensional umbrella sampling than with the already efficient multidimensional hills method, (2) the often difficult problem of choosing a good one-dimensional reaction coordinate is facilitated by allowing for the independent treatment of relatively simple collective variables in the hills method from which a good reaction is generated a posteriori (namely, the LFEP) to be used in the umbrella sampling, and (3) the second stage umbrella sampling repairs eventual imperfections introduced in the first stage hills method due to poor tuning of the hills method parametrization or violation of the requirement that the dynamic ionic and collective variable subsystems should be adiabatically decoupled.

The paper is organized as follows. Section II describes the hills method, the method used to localize the lowest free energy reaction path, and the umbrella sampling scheme that uses the LFEP. Section III presents our main results, where we apply this three-step scheme to the fundamental S_N2 reaction between Cl^- and CH_3Cl, once using a single reaction coordinate and once using two coordinates (collective variables) to compute the free energy surface. The following section IV is rather technical and is particularly aimed to guide users of the hills method. Here, we will use the converged result from section III to find optimal settings for the hills method's tuning parameters, such as the size and shape of the hills and the frequency of adding them to the biasing potential. Readers not interested in such technical detail can skip section IV. In the conclusions (section V), we summarize our findings and present a recipe for efficient computation of free energy profiles and reaction paths for intrinsically multidimensional transformations.

II. Methods

A. Hills Method. The aim of the hills method is to efficiently explore the free energy surface $F(\mathbf{s})$ of a limited set of collective variables s_α (e.g., bond lengths, angles, coordination numbers, etc.). The free energy is commonly written as

$$F(\mathbf{s}) = - k_B T \ln[Z(\mathbf{s})] \tag{1}$$

with k_B Boltzmann's constant, T the absolute temperature, and Z the partition function

$$Z(\mathbf{s}) = \frac{1}{Z} \int d\mathbf{r}\, e^{\mathscr{H}(\mathbf{r})/k_B T}\, \delta(s(\mathbf{r}) - s') \tag{2}$$

with $\mathscr{H}(\mathbf{r})$ the Hamiltonian. The delta function can be replaced

by an exponential

$$Z(\mathbf{s}) = \lim_{k \to \infty} \frac{1}{N_k} \frac{1}{Z} \int d\mathbf{r}\, e^{\mathscr{H}(\mathbf{r})/k_B T}\, e^{-k(s(\mathbf{r}) - s')^2} \tag{3}$$

Molecular dynamics simulation is used to evaluate this integral and to enhance the sampling over *s*; we introduce a fictitious particle s_α for each collective variable and employ an extended Lagrangian technique. The present example utilizes density functional theory (DFT)-based electronic structure calculations via Car–Parrinello molecular dynamics[28] (CPMD). The augmented Lagrangian is thus

$$\mathscr{L} = \mathscr{L}_{CPMD} + \sum_\alpha \frac{1}{2} \mu_\alpha \dot{s}^2_\alpha - \sum_\alpha \frac{1}{2} k_\alpha (S_\alpha(\mathbf{r}) - s_\alpha)^2 - V(t,\mathbf{s}) \tag{4}$$

The second term on the right-hand side is the total kinetic energy of the fictitious particles, which for large enough masses μ_α are adiabatically separated from the ionic and electronic degrees of freedom. Each fictitious particle s_α is connected to its actual collective variable $S(\mathbf{r})$ by a harmonic spring. For large enough force constants k_α, the springs restrain the molecular configuration close to the slowly moving particles s_α. The total potential energy of the harmonic springs gives rise to the third right-hand-side term in eq 4. The last term is the history-dependent biasing potential[25]

$$V(t,\mathbf{s}) = \sum_{t_i < t} H \exp\left[-\frac{(\mathbf{s} - \mathbf{s}^i)^2}{2(\Delta W^\perp)^2} \right] \exp\left[-\frac{((\mathbf{s}^{i+1} - s^i)(\mathbf{s} - s^i))^2}{2(\Delta W_i^{\parallel})^4} \right] \tag{5}$$

where $\mathbf{s}^i = \{s_\alpha(t_i)\}$. $V(t,\mathbf{s})$ describes a slowly growing discretized multidimensional Gaussian tube, with its axis along the trajectory. This biasing potential is a sum of repulsive Gaussian-shaped potential *hills*, each with height H (although in the original paper[25] H is an adaptive parameter that adjusts to the underlying energy landscape during the simulation). In eq 5, the first spherical Gaussian, with width $\Delta W^\perp$, is multiplied with a second Gaussian, with a width $\Delta W_i^{\parallel} = |s^{i+1} - s^i|$ that thus depends on the displacement between the potential hills added at t_i and t_{i+1}, such that subsequently added potential hills close to each other are narrowed in the direction of the trajectory.

In practice, one starts a simulation without adding hills so that $V(t,\mathbf{s}) = 0$ and the molecular system and the fictitious particles fluctuate in one of the free energy wells, e.g., the reactant well. The fluctuations of s_α give an indication of the width of the well from which the width $\Delta W^\perp$ of the Gaussian hills can be chosen. The *meta*dynamics of s_α determines the efficiency at which the free energy surface is being explored. Then, potential hills are added to the history-dependent potential, $V(t,\mathbf{s})$, with a meta-time step that is one or two orders larger than the MD time step. The potential discourages the system to revisit points in configurational space and rapidly builds up in the reactant state, until it counter-balances the underlying free energy well so that the system can escape via the lowest transition state to the next local (product) minimum. When all the local free energy minima are "filled up" with hills, the system can move freely from the reactant state to the product states. Continuing with smaller hills (H_i) results in better resolution so that the multidimensional free energy surface $F(\mathbf{s})$ is obtained to arbitrary accuracy as the negative of $V(t,\mathbf{s})$.

B. Localizing the Lowest Free Energy Path. From the N-dimensional free energy surface obtained from a simulation using the hills method, we locate the minima associated with
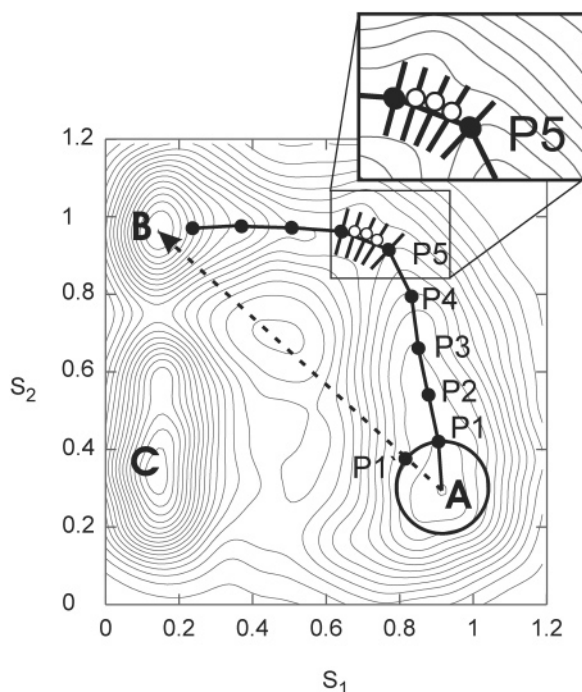
Figure 1. Finding the lowest free energy path on a 2D free energy surface from state A to state B, first by taking steps larger than the local bumpiness leading to points p_1, p_2, ..., and in the second step refining the path by optimizing points in between these points, perpendicular to the coarse path (as shown in the inset).

the stable reactant and product states as well as the connecting lowest free energy reaction paths. Figure 1 shows an illustrative contour plot of a 2D free energy surface as a function of two collective variables s_1 and s_2. The reactant well is denoted A, and the two product wells are labeled B and C. Locating the lowest free energy path (LFEP) that connects states A and B, for example, starts with finding the two minima. Good guesses for the locations of the minima s_A and s_B are readily obtained from the collective variable dynamics during the hills method simulation, as the collective variables spend most of the time fluctuating around these locations while the minima are being "filled up" with hills. Since the free energy surface can be locally bumpy depending on the convergence of the hills method and the size and shape of the potential hills used, computing the derivative $\partial V(\mathbf{s})/\partial s_\alpha$ is not very useful. Instead we minimize $V(\mathbf{s})$ starting from the initial guess, by choosing a bracket $[s_\alpha - \delta s_\alpha, s_\alpha + \delta s_\alpha]$ for which $V(s_\alpha) < V(s_\alpha - \delta s_\alpha)$ and $V(s_\alpha) < V(s_\alpha + \delta s_\alpha)$ ($V(\mathbf{s})$ is computed from eq 5). A new point s'_α is chosen between the initial point s_α and the bracket end $s_\alpha \pm \delta s_\alpha$ with the largest potential using the "golden section method".[29] If $V(s_\alpha) < V(s'_\alpha)$, then s'_α replaces the bracket end with the lower potential, otherwise s_α replaces the bracket end with the higher potential and s'_α becomes the improved minimum s_α. This is repeated by again taking a new point s'_α and so forth until $V(s_\alpha) - V(s'_\alpha)$ is smaller than some tolerance V_{TOL}. Convergence is reached through cycling over all collective coordinates α, repeating the minimization until $V(s_\alpha) - V(s'_\alpha) < V_{TOL}$ for all α.

Locating the lowest free energy path from A to B occurs in two steps. From A, first a coarse path is traced, with a step size larger than the local bumpiness (i.e., the resolution used in the hills method to compute the N-dimensional free energy surface) in the free energy surface. This is illustrated in Figure 1 by the circle with radius "step size" around the starting minimum. As our initial guess for the first point on the path, we take the

direction of the vector $\overline{AB}$ (the dashed arrow), which leads to point p'_1 on the circle. Then a similar minimization follows using the bracket method described above, but now constrained to the circle, by scaling back each new (bracket) point to be on the circle. This leads to our first point on the path p_1, which is then taken as the starting point for the next point by taking again a step in the direction of the vector $\overline{p_1 B}$, etc. If the minimization from p'_2 leads back to A, then alternatively a step in the direction of the vector $\overline{Ap_1}$ from p_1 is taken. This process results in a coarse path from A to B. In the second step, the path is refined by optimizing points between the coarse line segments in the direction perpendicular to the path as shown in the inset in Figure 1. The resulting parametrized path $\sigma^t(\mathbf{s})$ is the lowest free energy path in collective variable space and for a good choice of collective variables is also a good approximation of the lowest free energy path in the molecular configurational space.

The potential along the points $V(\sigma^t)$ already gives a good estimate for the one-dimensional free energy profile of the lowest free energy path in most cases. To find the correct free energy profile however, we have to take into account the width of the "valley" through which the path winds, by integrating the potential over the dimensions perpendicular to the path. This is readily done by performing an umbrella sampling Monte Carlo simulation in the reduced N-dimensional collective variable space (with the sum of hills $V(\mathbf{s})$ as the underlying free energy surface), using $V(\sigma^t)$ as the biasing umbrella potential. The trace_irc program to localize the minima and the connecting lowest free energy path after a hills method simulation can be downloaded free of charge from http://www.cmm.upenn.edu/~ensing/software. The resulting free energy profile $F(\sigma^t)$ will be used as input to perform umbrella sampling as explained in the next section.

C. Umbrella Sampling. Once we have a reasonable estimate of the free energy profile along the lowest free energy path $F(\sigma^t)$, we can use it as the umbrella potential $U(\sigma^t)$ to perform one-dimensional umbrella sampling to enhance the sampling of the activated reaction. Umbrella sampling has advantages over the multidimensional hills method in that it converges the free energy more efficiently and that it needs less detailed attention to perform at maximum efficiency and accuracy. The final free energy profile after umbrella sampling is recovered from

$$F(\sigma^t) = -U(\sigma^t) - k_B T \ln[P(\sigma^t)] + \text{const} \qquad (6)$$

$$P(\sigma^t) = \frac{1}{Z} \int d\mathbf{r} \, e^{(\mathcal{H}(\mathbf{r}) + U(\sigma^t))/k_B T} \, \delta(\sigma^t(\mathbf{s}(\mathbf{r})) - \sigma'') \qquad (7)$$

with $P(\sigma^t)$ the probability to find the system at σ^t. To apply the umbrella potential to our molecular system during an MD simulation, we have to compute the forces on the atoms due to the umbrella

$$f_i^U = \frac{\partial U(\sigma^t)}{\partial r_i} = \sum_\alpha \left(\left\{ \frac{\partial U(\sigma^t)}{\partial \sigma^t} \frac{\partial \sigma^t}{\partial s_\alpha} \right\} \frac{\partial s_\alpha}{\partial r_i} \right) \qquad (8)$$

The derivatives of the potential with respect to the collective variables $\nabla_{s_\alpha} U$ (i.e., the part between curly brackets in eq 8) are computed a priori (after localizing the LFEP and smoothing the path $\sigma^t(\mathbf{s})$ and the potential $U(\sigma^t)$ to remove spurious bumpiness; see also the previous section) and are read in from a file, together with the index t and the collective variables parametrizing the path $\mathbf{s}^t$, at the start of the umbrella sampling simulation. During the umbrella simulation at each time step,

Computations for Concerted Reactions

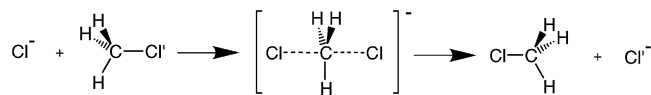*J. Phys. Chem. B, Vol. 109, No. 14, 2005* **6679**

Figure 2. S_N2 reaction between Cl^- and CH_3Cl showing the symmetric transition state and the CH_3 conversion of configuration known as the Walden inversion.

the system finds itself at the reaction coordinate value σ^t for which $|s(r) - s^t|$ is minimal so that $\nabla_{s_\alpha}U$ can be looked up and multiplied by $\partial s_\alpha/\partial r_i$ to obtain the forces on the atoms (see further details in the appendix). Additionally, we can divide the potential into overlapping windows to make the sampling of σ^t more efficient and to allow for parallel sampling.

D. Simulation Details. The computer simulations were performed using the Car–Parrinello molecular dynamics (CP-MD)[28,30] algorithm as implemented in the CPMD program.[4] A fictitious mass of $\mu_e = 600$ au was used for the electron coefficient dynamics, which allows for a MD time step of 5 atu (0.12 fs). The electronic structure was computed within the density functional theory (DFT) level of theory using the popular Becke, Lee, Yang and Parr (BLYP)[31,32] gradient corrected (GGA) exchange-correlation functional. The frozen core approximation was applied for the 2s electrons of second row elements and up to 3s for Cl. Troullier–Martins[33] pseudopotentials were used for the valence electrons, and the wave function was expanded in a plane waves basis set up to an energy cutoff of 70 Ry. A cubic supercell of length $L_{box} = 18$ au was used. The interaction between periodic images, due to the periodicity of plane waves, was canceled using an isolation technique.[34]

It is well-known that current GGA functionals underestimate the intrinsic reaction energy barrier of S_N2 reactions,[35,21] due to a spurious delocalization of the exchange hole over the three (attacking, central carbon, and leaving) atoms in combination with a very small nondynamical correlation in the transition state structure. Although hybrid functionals (i.e., DFT exchange functionals that mix in exact Hartree–Fock exchange) often show better performance for this notorious case, they cannot yet be used in combination with a plane wave basis set as is the case in CPMD. We nevertheless chose to test our method with the S_N2 reaction, because it is such a well-known test case and we are only interested in showing the efficiency and convergence of obtaining the reaction path and free energy surface at the DFT-GGA level of theory.

III. Application: S_N2 Reaction between Cl^- and CH_3Cl

Almost all free energy methods require some chemical intuition from the user, e.g., to find order parameters that define the stable states or, as in the traditional methods, define a reaction coordinate. In many cases, this is an important and unsolved problem. The proposed three-step scheme (hills method, LFEP localization, and 1D umbrella sampling) reduces the problem of finding a reaction coordinate significantly, which is illustrated by applying the scheme to the prototype S_N2 reaction.

The S_N2 reaction, shown in Figure 2 for the reaction between Cl^- and CH_3Cl, is a well-understood fundamental organic reaction, ideal to test our free energy method. The free energy profile is symmetric in this particular example because the products are the same as the reactants, which provides an additional check for the performance of our free energy method. The bonds made and broken are (obviously) the two C–Cl bonds. A good reaction coordinate in general is one that describes a reversable path between the stable reactant and
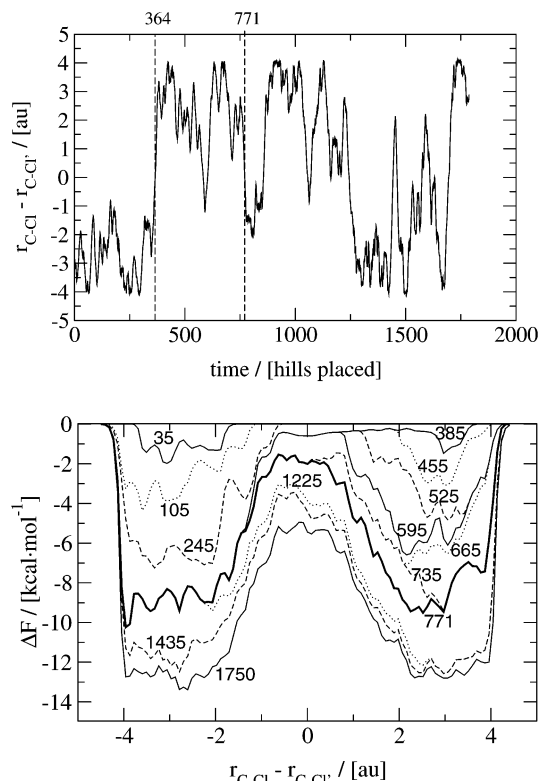

Figure 3. Upper panel: Dynamics of the single collective variable, $r_{C–Cl} - r_{C–Cl'}$ as a function of the number of potential hills added to the system (i.e., meta-time steps). After the addition of 364 hills to the system, the reactant well is filled, and the system moves to the product side. After 771 hills, the product well is also filled, and the system can freely move back and forth. Lower panel: Buildup of the hills at different stages in the simulation. Note how the profiles become smoother after having added 771 hills and having switched to adding smaller hills.

product states and resembles the unstable mode in the transition state;[19] the difference between the two C–Cl bond distances, $r_{C–Cl} - r_{C–Cl'}$, is such a reaction coordinate. However, often identification of a reaction coordinate is a problem, and in such a case the hills method facilitates the problem because it allows for the independent treatment of the relevant collective variables, in this case the two C–Cl bond distances. A good reaction coordinate can then be located a posteriori and, for example, applied in a traditional free energy method.

We performed two simulations of this system using the hills method. In the first simulation, the difference of the C–Cl distances was taken as a single collective variable. In the second simulation, the two C–Cl bond distances were treated independently as two collective variables. The one-dimensional free energy profiles were converged with umbrella sampling.

A. Hills Method Using One Collective Variable. Figure 3 shows the dynamics of the "difference of C–Cl distances" collective variable during the first hills method simulation. The mass of the collective variable, μ_α, was 10 amu, and the force constant of the spring, k_α, was 0.05 au (eq 4). Phase space boundaries in the form of repulsive potentials located at $r_{C–Cl} - r_{C–Cl'}$ values equal to -4.0 and 4.0 au prohibited the attacking Cl and the leaving Cl′ to escape. Initially the width and height of the Gaussian-shaped potential hills were set to $\Delta W^\perp = 0.15$ au and $H = 0.0005$ au (0.314 kcal/mol), respectively. Figure 3 shows that after adding 364 hills the system escapes from the reactant well over the transition state barrier to the product side of the reaction. After a total of 771 hills, the product well is also "filled with hills", and the system recrosses back to the
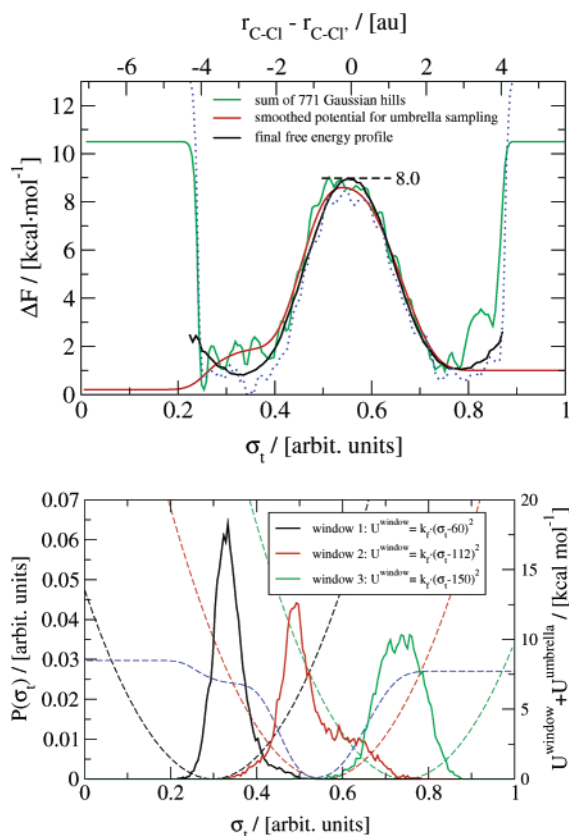
Figure 4. Upper panel: Free energy profiles as a function of the collective variable $r_{C-Cl} - r_{C-Cl'}$ (top axis) and along the parametrized LFEP (bottom axis), resulting from the accumulated 771 hills (green curve), after smoothing the hills curve (red curve), which is used as the biasing potential for the umbrella sampling, and the final result after umbrella sampling (black curve). Note that even after adding 1750 hills (blue dotted curve) convergence to the final result has not yet been reached. Lower panel: The probability plots resulting from the umbrella sampling over three windows (solid lines and left-hand-side axis) and the corresponding harmonic window potentials (dashed lines and right-hand-side axis) as well as the umbrella potential (blue dashed line).

reactant side. The free energy profile obtained from these 771 hills is shown by the bold black line in the lower panel in Figure 3 of the gradual buildup of the biasing potential. After having "filled up" the reactant and product wells, we continue the hills simulation using smaller hills ($H = 0.0002$ au (0.126 kcal/mol)). Note how the subsequent free energy profiles (i.e., of more than 771 hills) are less "bumpy" than the earlier ones in Figure 3 and mainly shift the overall profile downward compared to the one with 771 hills, without changing the general features.

B. Umbrella Sampling Using the 1D Hills Method Result. The profile obtained from 771 hills, which is after having "filled up" the reactant and product wells (and (re-)crossing the transition state only once), is used to construct the biasing potential for an umbrella simulation. Since we only have a one-dimensional free energy surface, we do not yet need to use the search algorithm described in section II.B to locate the LFEP; instead we parametrize the LFEP, σ_t, taking 200 equidistant points along the single collective variable. This reaction coordinate is a measure of the progress of the reaction, which we choose to start at $\sigma_t = 0$ somewhat "before" the actual reactant well minimum and end at $\sigma_t = 1$ somewhat "after" the product minimum, as shown at the lower x-axis in Figure 4. The corresponding collective variable, $r_{C-Cl} - r_{C-Cl'}$, is taken as the additional top horizontal axis. The green curve shows again the free energy profile constructed from 771 Gaussian
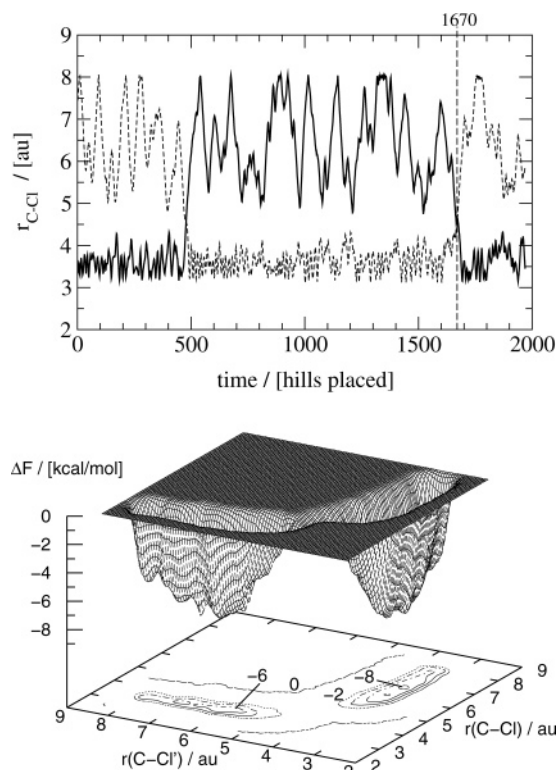

Figure 5. Upper panel: Dynamics of the two collective variables, r_{C-Cl} and $r_{C-Cl'}$, as a function of the number of potential hills added to the system. After the addition of 1670 hills to the system, both the reactant well and the product well are filled. Lower panel: Free energy surface after adding 1670 hills.

hills. The red curve, which is used for the umbrella sampling biasing potential, shows this profile after smoothing, by taking a Gaussian weighted running average. Since we are only interested in increasing the probability of visiting the transition state by umbrella sampling but not the probability of visiting the outer regions, we set the biasing potential at the regions outside the local minima equal to the value of the local minima (red curve). Three harmonic potentials, centered at $\sigma_t = 60$, 112, and 150 with a force constant equal to $k_f = 6 \times 10^{-6}$ au were applied to divide the sampling of the LFEP up into overlapping windows in order to speed up the umbrella sampling. The resulting probability functions (eq 7) are shown in the lower panel of Figure 4. The free energy profile was recovered using the weighted histogram analysis method (WHAM)[36] and is shown by the black line in the upper panel of Figure 4. Comparing the free energy profiles obtained with the hills method with those from the umbrella sampling result shows that the profile constructed from 771 Gaussian hills (green line) is in qualitative agreement with the umbrella sampling benchmark. The sum of 1750 hills (dotted blue line) shows better comparison with the umbrella sampling result but still exhibits bumps in the profile of about 1 kcal/mol, even though the height of the last thousand Gaussian hills was set to 0.126 kcal/mol. Comparing the computational cost of the two methods is difficult, since the total simulation time of 30 ps for the hills simulation (1750) was much shorter than the 50 ps simulation time per window for the three umbrella sampling simulations, but the convergence for the free energy profile is much better for the umbrella sampling compared to that for the hills method.

C. Hills Method Using Two Collective Variables. The result for the second, now two-dimensional, hills method simulation is shown in Figure 5. Again we start by adding Gaussian hills with a height of 0.314 kcal/mol but now switch to adding the
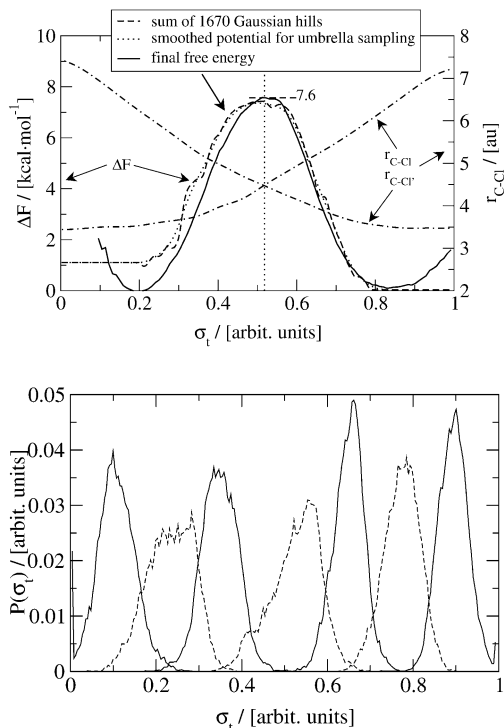
Computations for Concerted Reactions

J. Phys. Chem. B, Vol. 109, No. 14, 2005 **6681**

Figure 6. Upper panel: Free energy profiles as a function of the parametrized LFEP resulting from the accumulated 1670 hills (dashed curve), after smoothing the hills curve (dotted curve), and the final result after umbrella sampling (sollid curve). The dot−dashed lines show the C−Cl distances along the LFEP (using the right-hand-side axis). The LFEP value where the r_{C-Cl} lines cross is emphasized by the vertical dotted line to accentuate the symmetry in the free energy profile that is only recovered after umbrella sampling. Lower panel: The probability plots resulting from the umbrella sampling using seven overlapping windows.

smaller 0.125 kcal/mol hills after the system crosses the transition state (where the two C−Cl bond distances are equal) to the product side, after roughly 500 hills. Due to the higher dimensionality of the free energy surface of the second run compared to the first run, it takes many more hills (500 versus 364) to fill up the reactant well. After the continuation of the addition of the smaller hills, it takes another 1170 hills to fill the product well, after which the system recrosses to the reactant state. However, as expected, using the smaller hills results in a much smoother free energy surface as seen by comparing the product well with the reactant well in the lower panel in Figure 5. Moreover, the bumpiness of the reactant well led to a premature escape from the reactant well so that the reactant well is predicted to be not as deep as the product well.

D. Umbrella Sampling Using the 2D Hills Method Result. The lower reactant well depth compared to the product well depth mentioned previously becomes more apparent after we locate the lowest free energy path, σ_t, in the 2D free energy surface and plot the free energy along σ_t, as shown by the dashed line in Figure 6. The umbrella sampling was performed using the smoothed sum of 1670 hills as the biasing potential (dotted line) and parallelized by dividing the sampling of σ_t into seven overlapping windows, using harmonic potentials with a force constant of $k_f = 2.5 \times 10^{-6}$ au centered at $\sigma_t = 20$, 55, 90, 125, 160, 195, and 230. After umbrella sampling, we recover the symmetric free energy profile (solid line) and see that the product well estimate using the smaller hills is in rather good comparison, whereas the reactant well depth is underestimated by the sum of larger hills. The final result of the 2D calculation compares very well with that of the 1D calculation (compare

TABLE 1: Average Fluctuation of the Collective Variable s_α around the Instantaneous Coordinate $S(\mathbf{r})$ for Different Values of the Force Constant k_α

k_α/au	$\langle(s_\alpha - S(\mathbf{r}))^2\rangle/a_0^2$
0.0001	1.99
0.05	0.010
0.1	0.0048
1.0	0.00058

Figure 4 to Figure 6). The barrier heigh of 7.6 kcal/mol in the 2D case is slightly lower than the 8.0 kcal/mol barrier of the 1D calculation, which is probably due to the more confined minima along σ_t in the 1D case compared to the 2D case.

IV. Fine-Tuning the Hills Method

The examples of the S_N2 reaction in the previous sections demonstrated, in the first place, that we can explore the relevant regions of a multidimensional free energy surface very efficiently using the hills method and, in the second place, that we can compute the free energy profile along the lowest free energy reaction path very accurately using an umbrella sampling scheme. Using the umbrella sampling result for the S_N2 reaction as a reference, we will now focus our attention on the performance of the hills method. Two factors that are key to the performance are (1) the collective variable dynamics that determines the efficiency of the FES exploration (examined in the next subsection) and (2) the buildup of the history-dependent biasing potential that determines the convergence of the free energy profile (section IV.B).

A. Metadynamics of the Collective Variables: Choosing μ_α and k_α. The dynamics of the collective variables, s_α, governed by the equations of motion derived from eq 4, is controlled by the masses, μ_α, and the force constants, k_α. The force constants have to be chosen large enough to keep s_α close to the actual coordinates of the system, $S(\mathbf{r})$, which is

$$\langle(s_\alpha - S(\mathbf{r}))^2\rangle \ll \langle(S(\mathbf{r}) - S^\circ)^2\rangle \qquad (9)$$

with S° the minimum of the well. However, a large value for k_α requires a small time step for the integration of the equations of motion, which makes the simulation more computationally demanding.

Table 1 shows the fluctuations $\langle(s_\alpha - S(\mathbf{r}))^2\rangle$ as a function of the force constant for the $[Cl^- \cdots CH_3Cl]^-$ complex, using a collective variable with a mass of $\mu_\alpha = 100$ amu attached to the "difference of C−Cl distances" coordinate (without adding potential hills). The fluctuations of this coordinate in the reactant well are $\langle(S(\mathbf{r}) - S^\circ)^2\rangle \approx 1.2a_0^2$ at $T \approx 300$ K. Clearly, a force constant of $k_\alpha = 0.0001$ does not yield meaningful values for s_α because its deviations from the actual coordinate value, $S(\mathbf{r})$, are even larger than the well size. On the other side of the spectrum, i.e., for a simulation using $k_\alpha = 1.0$ and a time step of 4 au, the total energy is not conserved. The values $k_\alpha = 0.1$ and $k_\alpha = 0.05$ are useful because the fluctuations $\langle(s_\alpha - S(\mathbf{r}))^2\rangle$ are small and the total energy remains conserved. Table 1 also shows that the fluctuations are inversely proportional to k_α. In fact, under the condition of adiabatic separation, if the atomic system is kept at a temperature T, then the average value of $1/2(s_\alpha - S(\mathbf{r}))^2$ is equal to $1/2 k_B T$, hence

$$\langle(s_\alpha - S(\mathbf{r}))^2\rangle = \frac{k_B T}{k} \qquad (10)$$

Having established a range of useful k_α values, we will choose the mass μ_α next. Since the general idea of having the fictitious
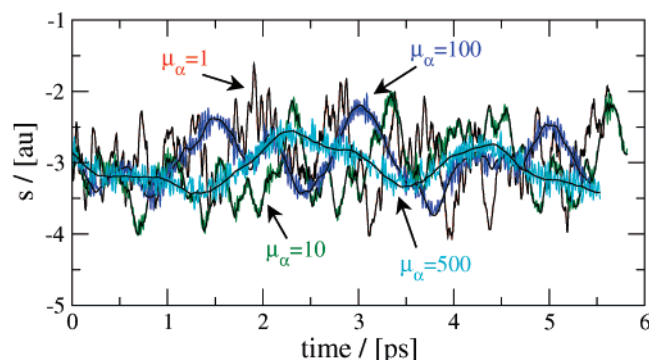
Figure 7. Dynamics of $S(\mathbf{r}) = r_{C-Cl} - r_{C-Cl'}$ (red, $\mu_\alpha = 1$ amu (mostly hidden behind the black s_α line); green, $\mu_\alpha = 10$ amu; blue, $\mu_\alpha = 100$ amu; cyan, $\mu_\alpha = 500$ amu) and the fictitious particle s_α (black lines) of the $[Cl^- \cdots CH_3Cl]^-$ complex using different masses μ_α.

collective variables within the hills method is to have a slow and heavy particle that "rolls" over the rugged free energy landscape, while the relatively fast molecular motions sample the perpendicular directions, μ_α should be relatively large, and the collective variable dynamics ideally should be adiabatically decoupled from the atomic motions.

In practice however, we have found that the use of large enough values for μ_α to ensure adiabatic decoupling makes the exploration of the free energy surface very slow and computationally demanding in combination with CPMD. This means that we have to focus on finding a satisfactory balance between minimal energy flow between the electronic, ionic, and collective variable dynamics subsystems on one hand and a workable efficiency in free energy surface exploration on the other. Coupling between the collective variable dynamics subsystem and the relatively cool electronic dynamics subsystem should nevertheless be avoided at all cost, because heating-up of the latter causes the electronic wave function to deviate from that of the ground state, which leads to erroneous forces between the ions. We will however tolerate a minor nonadiabicity between ions and collective variable dynamics subsystems for the benefit of efficiency. This is allowed in our dual scheme, because possible small deviations in the free energy surface will be repaired in the umbrella sampling step. Note also that a certain heating-up of the ionic subsystem cannot be avoided when adding hills, due to the fact that potential energy is added to the system with every hill that we add to the biasing potential. The collective variables continuously pull on the ionic system as they always roll down a hill. This effect is minimized by controlling the temperature of both subsystems to fluctuate around the same target value. For now, we will concentrate on how to minimize the coupling between the subsystems and in the next section, when we start adding hills, focus on the efficiency in exploring the free energy surface as a function of the chosen mass μ_α.

The effect of the mass on the collective variable, $S(\mathbf{r})$, and its fictitious particle, s_α, is illustrated by Figure 7, showing the results for four simulations of the $[Cl^- \cdots CH_3Cl]^-$ complex using the difference of C–Cl distances variable, $S(\mathbf{r}) = r_{C-Cl} - r_{C-Cl'}$. The spring constant was $k = 0.05$ au.

For the small mass $\mu_\alpha = 1$ amu, the motion of the fictious particle s_α is much faster than the vibration of $S(\mathbf{r})$ (contrary to the idea behind the hills method). As we go to larger and larger masses, the frequency of s_α decreases and deviates more and more from the relatively fast $S(\mathbf{r})$ frequency. Note also that the amplitude of the s_α oscillations in the reactant well decrease with increasing μ_α. From a frequency analysis of the metadynamics Hamiltonian, we can derive that the period of the motion
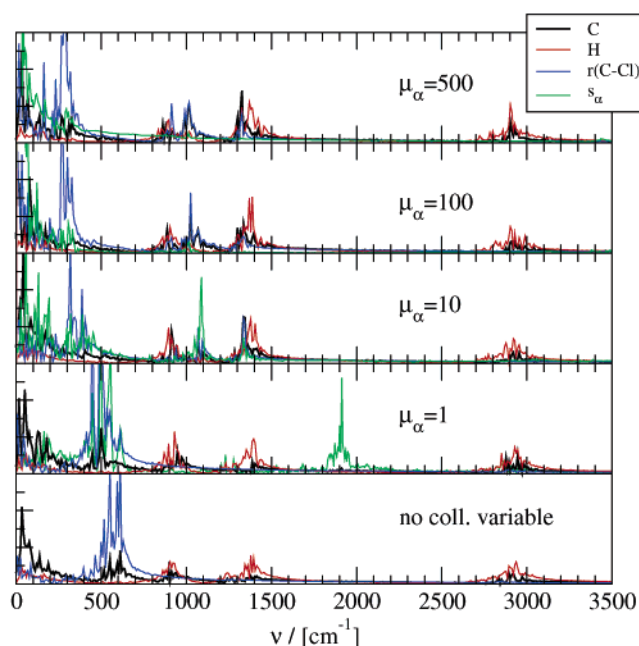

Figure 8. Vibration spectra of the $[Cl^- \cdots CH_3Cl]^-$ complex using different masses for the collective variable (from top to bottom $\mu_\alpha = 500, 100, 10, 1$ amu and without a collective variable shown at the bottom).

of the collective variables around a stable state equals

$$\tau_\alpha = \sqrt{\frac{\mu_\alpha}{k_\alpha}} \qquad (11)$$

Ideally, we want this frequency to be much lower than the frequencies of the intramolecular vibrations. Figure 8 shows the vibration spectra of four simulations with the different masses plus the result of a simulation of the $[Cl^- \cdots CH_3Cl]^-$ complex without the collective variable dynamics (bottom panel.) For the small mass $\mu_\alpha = 1$ amu, we find a s_α peak at 1900 cm^{-1}, between the C–H symmetric and antisymmetric stretch vibrations. Other peaks appear around $\nu = 600$ cm^{-1} as s_α follows the C–Cl bond stretch vibration. From eq 11, we know that there is an even faster vibration at 7191 cm^{-1} that is very likely to interfere with the electronic dynamics. The splitting of the C–Cl bond stretch vibration around $\nu = 600$ cm^{-1} (lower panel) into higher and lower vibrations (upper three panels) is due to the coupling of this vibration with the other, slower intermolecular C–Cl vibration via the spring attached to s_α. The spectrum from a simulation using $\mu_\alpha = 5000$ amu is very similar to that of $\mu_\alpha = 500$ amu and therefore not shown. For $\mu_\alpha = 100$ amu and larger, we see that the s_α vibration shifts below the lowest intramolecular vibrations shown in the lowest panel. Clearly mass values smaller than $\mu_\alpha = 100$ amu should be avoided for this system.

B. Convergence of the Free Energy Surface: Choosing H, $\Delta W^\perp$, and Δt. With sound metadynamics of the collective variables, as controlled by a proper choice of μ_α and k_α (section IV.A), the speed and accuracy of the buildup of the history-dependent biasing potential (i.e., the multidimensional free energy surface) are determined by the stride between added hills, Δt, and the height, H, and width, $\Delta W^\perp$, of the Gaussian-shaped hills. These three parameters cannot be chosen independently.

In the first place, the larger the size of the hills, the more time the system needs to relax before the next hill can be added, thus requiring a larger stride. A stride that is too small can lead to "hill surfing" as the collective variable continuously rides
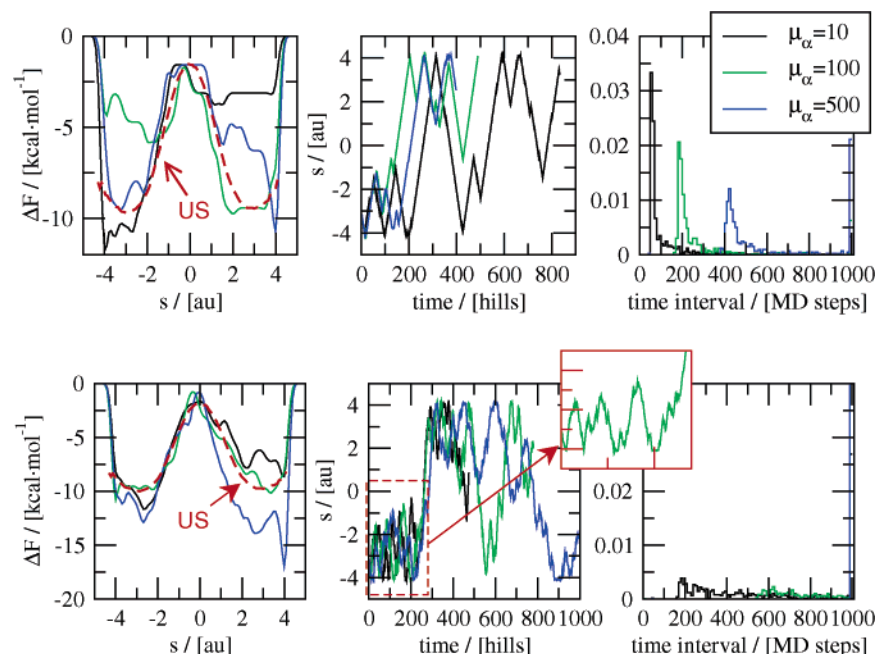
Computations for Concerted Reactions

J. Phys. Chem. B, Vol. 109, No. 14, 2005 **6683**

Figure 9. Left-hand-side plots: Buildup of hills after filling up the reactant and product wells compared to the umbrella sampling result (red dashed line) shown with different masses (black, $\mu_\alpha = 10$ amu; red, $\mu_\alpha = 100$ amu; blue, $\mu_\alpha = 500$ amu) for the collective variable and different distance criteria for the stride $\Delta S^{\min}$ (top-row plots, $\Delta S^{\min} = 1/2 W$; bottom-row plots, $\Delta S^{\min} = 3/2 W$. Middle plots: dynamics of the collective variable, s. Right-hand-side plots: Distribution of average number of MD steps between subsequent hills. The inset illustrates the slow oscillations of s as the reactant well is filled using $\mu_\alpha = 100$ amu.

the tail of the most recently placed hill, which leads to erroneous results. In the extreme case, the hills build up to a large spurious bump before the system can escape to energetically more favorable regions in collective variable space. However, too large a stride as well as hills that are too small lower the efficiency of the phase space exploration.

In the second place, the ratio between the hill height and hill width determines the "steepness" of the hill. The steeper the hill, the larger the forces on the collective variables due to the biasing potential. The maximum force due to a Gaussian-shaped hill equals

$$f^{\max} = -\frac{H}{\Delta W^\perp} e^{-1/2} \qquad (12)$$

Forces that are too large can lead to problems with the integration of the equations of motion so that larger masses for the collective variables or a smaller MD time step have to be chosen, which again lowers the efficiency of the sampling. Moreover, in the form of eq 5, the Gaussian hill is multiplied by a second Gaussian that narrows the (multidimensional) potential hill further in the direction of the displacement of the collective variable, which can lead to extreme forces in the case of small displacements of the collective variable. In our initial attempts to apply the hills method to the $S_N 2$ reaction, this led to very bumpy and rough free energy surfaces (e.g., Figure 3). In the following tests, we therefore do not apply the second Gaussian to narrow the hill (i.e., we use Gaussian hills of fixed size, independent of the collective variable dynamics), and second, we control the temperature of the collective variable by scaling the velocity down if the temperature becomes to high.

We will start by showing the dependence of the buildup of the hills potential on the stride, Δt. The system is again the one-dimensional $S_N 2$ reaction, and the size of the hills is fixed at $H = 0.314$ kcal/mol and $W = 0.15$ au. The efficiency and accuracy of the buildup is highly dependent on the velocity of the collective variable (i.e., the time it takes to glide down a

hill before the next hill can be added) so that we show the results for different masses, μ_α, of 10, 100, and 500 amu (Figure 9). The minimal time it takes for the collective variable with temperature T_α to travel a fraction f_W of the width of the hill is estimated by

$$\Delta t^{\min} = f_W W \sqrt{\frac{\mu_\alpha}{k_B T_\alpha}} \qquad (13)$$

For example, for subsequent hills to be separated by $1/2 W$, using $\mu_\alpha = 10$ amu and assuming $T_\alpha = T = 300$ K, the stride should be at least $\Delta t^{\min} = 329$ atu, which corresponds to 66 MD steps, using a CPMD time step of 5 atu. In the following, we apply a slightly more advanced stride, by demanding a minimal number of 50 MD steps and a minimal displacement from the previous hill $\Delta S^{\min}$ before adding the next hill. If the collective variable does not move by $\Delta S^{\min}$ within a maximum number of 1000 MD steps, then we also add a hill. In Figure 9, the top row of panels show the result using a distance criterion of $\Delta S^{\min} = 1/2 W$. The distribution of the time interval between subsequent hills (right-hand-side plot) indeed shows a maximum close to 66 MD steps for $\mu_\alpha = 10$ amu (and maxima at 208 and 465 steps for $\mu_\alpha = 100$ and 500 amu, respectively), following eq 13. By use of a distance criterion of $\Delta S^{\min} = 3/2 W$, the time interval distribution is flatter with a peak at 1000 MD steps using masses of 10 and 100 amu (bottom row, right-hand-side panel in Figure 9); for $\mu_\alpha = 500$ amu the time interval is always the maximum of 1000 steps (as expected from eq 13, $\Delta t^{\min} = 1400$ steps).

The average number of MD steps between subsequent hills, which results from our choice of mass and distance criterion, has important effects on the collective variable dynamics. That is that we see excellent behavior for the collective variable dynamics using $\Delta S^{\min} = 3/2 W$. For example, in the inset in Figure 9, the green line ($\mu_\alpha = 100$ amu) shows the variables slow motion around the reactant well minimum (its fast vibration

TABLE 2: Number of Hills and MD Steps Needed for the Metadynamics to Fill Up the 1D S_N2 Reactant and Product Wells (and Recross Back to the Reactant State) Using Different Masses μ_α, Distance Criteria ΔS^{min}, and Hill Dimensions, H (kcal/mol) and W (au)

ΔS^{min} (au)	μ_α (amu)	reactant well			product well		
		hills	MD steps ($\times 10^3$)	quality	hills	MD steps ($\times 10^3$)	quality
				$H = 0.314, W = 0.15$			
	10	259	41.5	reasonable	372	55.1	poor
0.075	100	150	48.9	poor	419	126.5	poor
	500	207	126.1	reasonable	>398	>238	poor
				$H = 0.314, W = 0.15$			
	10	260	147.9	reasonable	455	494.8	poor
0.225	100	263	234.2	good	517	464.2	good
	500	285	364.1	reasonable[a]	668	747.1	poor[a]
				$H = 0.314, W = 0.60$			
0.225	100	74	346.1	good	145	684.0	good
				$H = 0.628, W = 0.30$			
0.225	100	91	321.1	reasonable	208	747.5	poor

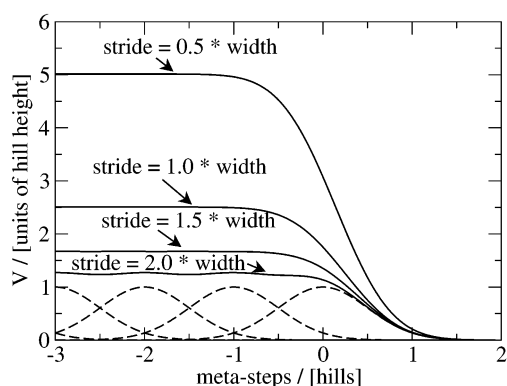[a] Poor quality is due to too small a maximum step criterion of 1000 MD steps.

Figure 10. Wave fronts resulting from accumulating hills that were positioned using different distance criteria. Using a distance of $\Delta = 0.5 \times \Delta W^\perp$ between subsequent hills results in a biasing potential that is 5 times higher than the hill height. As an example, the placement of the hills using a distance of $\Delta = 2 \times \Delta W^\perp$ is illustrated in dashed lines.

from the interaction with the harmonic spring is not well visible in this figure) with increasing amplitude until it escapes to the product side after three oscillations where it repeats the same behavior. After that, the collective variable recrosses the barrier back and forth. The sum of hills until the first recrossing, shown by the green line in the left-hand-side panel (i.e., after 517 hills and 464 200 MD steps, as listed in Table 2), shows close resemblance to the umbrella sampling result (red dashed line). However, the collective variable dynamics using $\Delta S^{min} = \frac{1}{2}W$ (top-middle panel) shows spiked dynamics, resulting in poor free energy surfaces (top-left panel). The latter erratic dynamics is the result of "hills surfing". The problem is illustrated in Figure 10, where we show the height of the "wave front" that results from partly overlapping hills as a function of the distance criterion. By the use of $\Delta S^{min} = \frac{1}{2}W$, the collective variable rides a wave that is at least five times higher than the hill height H. In practice, the front will be even higher due to the use of a maximum number of MD steps. In fact, the poor free energy profile in the case of $\Delta S^{min} = \frac{3}{2}W$ and $\mu_\alpha = 500$ amu (blue line in lower-left panel) is due to the use of a maximum number of 1000 MD steps. We thus recommend using a distance criterion of $\frac{3}{2}W$ (or larger but that would be less efficient) and a maximum number of MD steps criterion of at least 2 times Δt^{min} or using eq 13 with $f_W = \frac{3}{2}$ to calculate the minimal value for a fixed stride. Concerning the mass, values lower than $\mu_\alpha = 100$ amu easily cause dramatic nonadiabaticity problems

and require frequent quenching of the electron coefficient dynamics (section IV.A). Larger masses result in better collective variable dynamics (using an appropriate distance criterion and maximum number of MD steps criterion) but require more MD steps and computer time (Table 2). Keep in mind, however, that convergence of entropic contributions to the free energy profile requires careful sampling of many configurations, which is enhanced by the use of a larger mass.

Next, we show the effects of the width and height of the hills on the accuracy and efficiency of the calculation of the free energy profile. The area of a 1D Gaussian hill scales linearly with the width and height of the hill

$$A = \int_{-\infty}^{\infty} H \exp\left[-\frac{1}{2}\left(\frac{s}{W}\right)^2\right] ds = HW\sqrt{2\pi} \qquad (14)$$

It is thus tempting to assume that increasing the size of the hills will lead to faster buildup of the biasing potential and escape from the stable states. However, realizing that increasing the width requires an increase of the stride to avoid hill surfing and increasing the height requires increasing the width (and therefore the stride) or decreasing the MD time step to avoid problems with too large forces on the collective variables, we understand that the timings do not necessarily improve upon increasing of the hills size. The bottom rows of Table 2 show our results for a hills method simulation using a height and width of $H = 0.314$ kcal/mol and $W = 0.60$ au and for another simulation using $H = 0.628$ kcal/mol and $W = 0.30$ au. With the mass $\mu_\alpha = 100$ amu and the distance criterion $\Delta S^{min} = \frac{3}{2}W$, eq 13 tells us that we need a stride of at least 2.5×10^3 MD steps between subsequent hills (for $W = 0.60$ au), so we increased the maximum number of steps between subsequent hills to 5000. Indeed, in both cases longer simulation times were needed to fill up the reactant and product wells (684×10^3 and 747×10^3 MD steps, see last columns in the table) compared to that of the simulation using the smaller hills of $H = 0.314$ kcal/mol and $W = 0.15$ au (464×10^3 MD steps), even though the number of hills decreases with almost a factor of 4 as expected from eq 14 ($517/145 = 3.6$ for the case of $H = 0.314$ kcal/mol and $W = 0.60$ au; in the case of $H = 0.628$ kcal/mol and $W = 0.30$ au the ratio is lower because too many hills are added as discussed next). Figure 11 shows that the time interval between subsequent hills equals most often the maximum of 5000 in the simulations, which means that the anticipated minimum displacement of $\Delta S^{min} = \frac{3}{2}W$ is often not reached. The simulation using $H = 0.314$ kcal/mol and $W = 0.60$ au
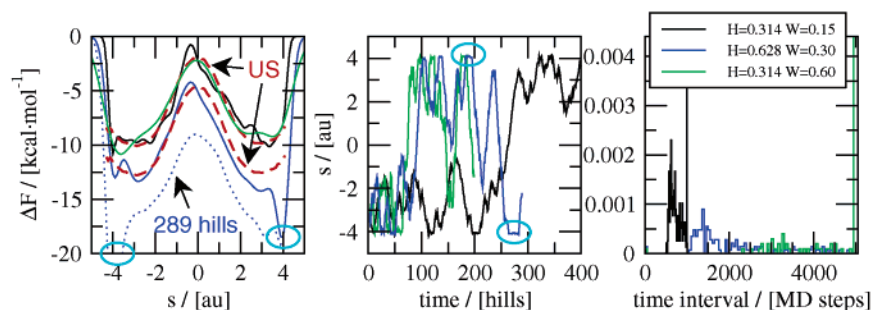
Figure 11. Left-hand-side plot: The free energy profile after having filled the reactant and product wells compared to the (arbitrarily shifted) umbrella sampling result (red dashed line) shown for different height H and width W of the hills (see legend). The distance criterion for the stride was $\Delta S^{min} = {}^{3}/_{2}W$. Middle plot: Dynamics of the collective variable. Right-hand-side plot: Distribution of average number of MD steps between subsequent hills. Light-blue circles indicate bumps in the $H = 0.628$ kcal/mol profile due to "sticking" to the confining repulsive walls (see text for further detail).
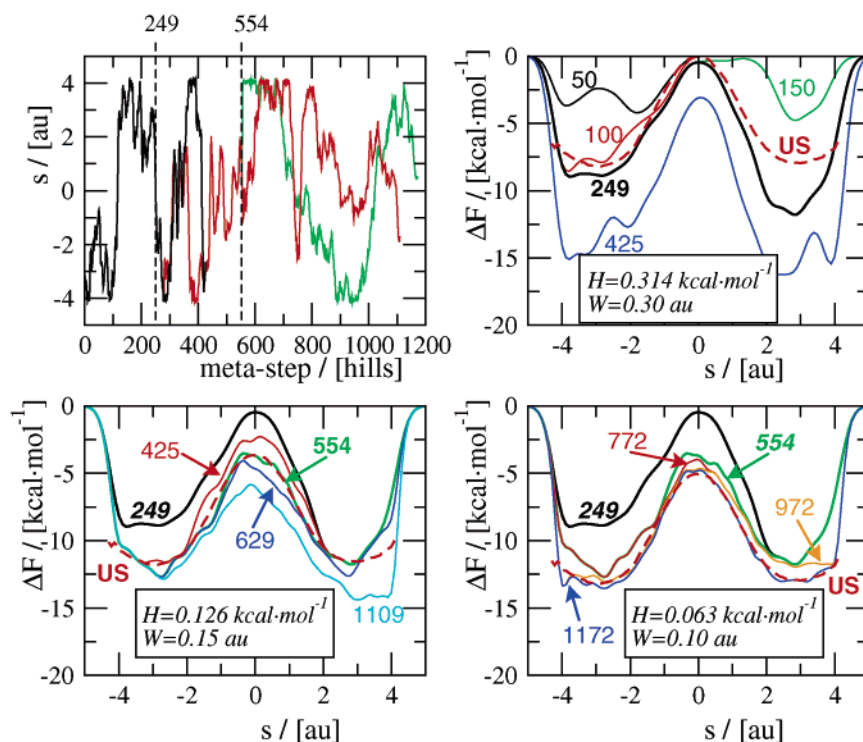

Figure 12. Convergence of the hills method to the umbrella sampling (US) result in three steps. Upper-left panel: Metadynamics of the collective variable while adding potential hills starting with a hill height $H = 0.314$ kcal/mol (black), switching to $H = 0.126$ kcal/mol (red) after 249 hills and switching finally to $H = 0.063$ kcal/mol after a total of 554 hills. Other three panels: Buildup of the free energy potential at different stages for the three hill heights compared to the US result (red dashed line). Profiles at the switching stages (249 and 554 hills) are bold.

(green lines) nevertheless results in a very reasonable estimate of the free energy profile. Note that the curve is smoother compared to the one using $W = 0.15$ (black line). However, using the higher $H = 0.628$ kcal/mol leads to a downward shift and decreased similarity to the umbrella sampling result of the free energy profile. The spikes at the reaction coordinate values of $s = -4$ and 4 au are due to the repulsive walls that we apply at these collective variable values to avoid too great a separation of the reactants. Apparently the collective variable "sticks" to these walls (see also the light-blue encircled regions in Figure 11), because the actual system travels beyond the wall before the spring pulls it back, so that in the meantime hills are being placed in the neighborhood of the wall that shut in the collective variable. This effect is enhanced by the use of a larger mass as was already visible in Figure 9 (note the spikes in the blue lines). Another effect that leads to decreased accuracy with increased hill height is that the ability of the hills method to self-heal artifacts in the free energy surface due to misplaced hills is

decreased by using higher hills, in particular when using hill heights larger than k_BT (0.628 kcal/mol $\approx 1k_BT$).

Finally, we attempt to illustrate the convergence of the free energy profile to the umbrella sampling result, with a hills method simulation using a fixed stride of $\Delta t = 250$ MD steps and a mass of $\mu_\alpha = 100$ amu. We start of with a hill size of $H = 0.314$ kcal/mol and $W = 0.30$ au. Figure 12 shows the metadynamics of the collective variable in the first panel and the buildup of the free energy profile at different stages during the simulation in the top-right panel. After the addition of 249 hills, both the reactant and the product wells are apparently filled, and the system recrosses to the reactant state; the resulting free energy profile at this stage is indicated by the bold black line. Note that continuation of the simulation with the same hill size to sample more recrossings and obtain better statistics does not improve the free energy profile (see the blue line after 425 hills). Instead we continue the simulation from the stage of 249 hills after decreasing both the hill height and width to H

$= 0.126$ kcal/mol and $W = 0.15$ au, as shown by the red line in the first panel and the buildup of the profile in the lower-left panel. Note how in this second part the simulation first repairs the asymmetry in the profile caused in the first part by adding hills from $s = -4$ to 2 au and then starts to fill in the dent close to $s = 4$ au. After adding a total of 554 hills, we decrease the hills size once more to $H = 0.063$ kcal/mol and $W = 0.10$ au until we find the free energy sufficiently converged after adding a total of 1172 hills in $1172 \times 250 = 293.00$ MD steps, much faster than any of the previous "good quality" hills method simulations shown in Table 2 and with a simulation time of 35 ps more efficient than the umbrella sampling simulation time of 3×50 ps.

V. Conclusions

The hills method is a powerful method to efficiently explore a multidimensional free energy surface, based on the buildup of a history-dependent repulsive biasing potential during a (Car−Parrinello) MD simulation. We have extended the hills method with an algorithm that locates the lowest free energy path connecting the reactant state with the product state in the free energy landscape obtained with a hills method simulation. The lowest free energy path indicates the most probable reaction mechanism followed during a (chemical) reaction, similar to the intrinsic reaction coordinate (IRC), but also includes the often important entropy (temperature) effects. Locating the lowest free energy path transforms the multidimensional problem of intrinsically concerted reactions back to a one-dimensional coordinate, which allows for the application of traditional free energy methods such as constrained MD, steered MD, and umbrella sampling.

We have applied the hills method to compute one- and two-dimensional free energy surfaces for the prototype S_N2 reaction between Cl^- and CH_3Cl. This example showed that the often difficult problem of choosing a chemically intuitive reaction coordinate is significantly reduced by the hills method because it allows for the independent treatment of relatively simple collective variables, for example, the lengths of the bonds that are broken and formed during the reaction. A posteriori, the lowest free energy path can be taken as a good reaction coordinate. Here, umbrella sampling was employed to converge the free energy profiles along the lowest free energy paths.

The converged 1D free energy profile obtained with umbrella sampling allowed for thorough testing of the hills method. This way, we are able to provide a range of parametrizations for which the hills method performs accurately and efficiently as well as identify parameter values that could lead to poor performance. In particular, nonadiabaticity, hill surfing, and the continuous addition of (potential) energy to the system with every added repulsive hill can lead to spurious metadynamics and erroneous results for the free energy surface.

We propose the following recipe for obtaining the reaction mechanism and free energy profile (i.e., the essential ingredients that describe a chemical reaction) for intrinsically multidimensional reactions. First, identify the relevant collective variables (bond distances, angles, torsion angles, coordination numbers) that describe the reaction and perform short metadynamics simulations without adding hills to obtain values for the mass and spring constants that guarantee healthy (largely adiabatically decoupled) metadynamics. The amplitudes of the collective variables in the reactant well indicate the width of the well, allowing for a hill width to be chosen. Second, perform the hills method simulation, using a hill height of $H = 0.2 - 2k_BT$ (depending on the desired accuracy versus sampling speed) and
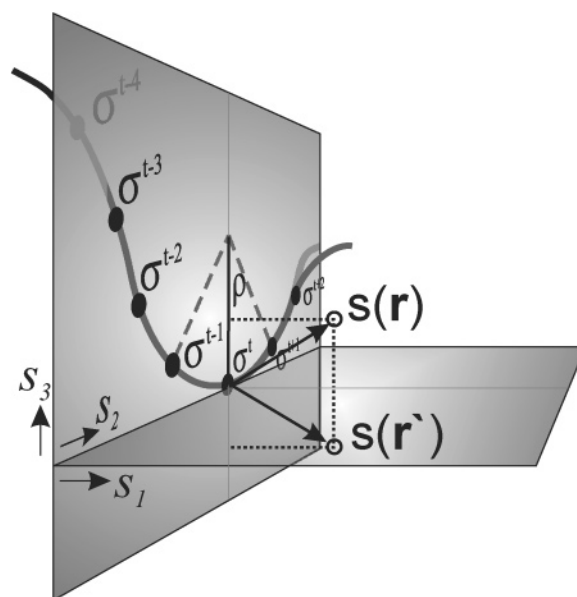

Figure 13. A curved parametrized path σ^t in 3D collective variable space, with two example points $\mathbf{s}(\mathbf{r})$ (open circles) of systems finding themselves at a reaction coordinate value σ^t. The local plane of curvature at σ^t is the one through σ^{t-1}, σ^t, and σ^{t+1} (i.e., the s_2s_3 plane in this case). The radius of curvature is ρ.

a displacement dependent stride Δt based on $^3/_2$ hill width or a fixed stride using eq 13. Decrease the hills size after every recrossing for free energy convergence. Third, locate the lowest free energy path to depict the reaction mechanism. Finally, perform one-dimensional umbrella sampling along the lowest free energy path to obtain the reaction free energy profile and reaction barrier to arbitrary accuracy.

Combining the hills method with umbrella sampling unites the efficient treatment of concerted multidimensional reactions with the straightforward and accurate calculation of a free energy profile along a 1D reaction coordinate. Moreover, the shift of the free energy convergence to the umbrella sampling part leaves less apprehension toward the fine-tuning of the hills method.

Appendix A: Derivatives $\nabla_{s_\alpha} U$ after Reduction to One Dimension

The umbrella sampling algorithm introduced in section II.C, requires the derivatives of the potential with respect to the collective variables $\nabla_{s_\alpha} U$ (the part between curly brackets in eq 8), which we take to be these derivatives at the parametrized lowest free energy path σ^t. This approximation is exact in the limit of the path $\sigma^t(s)$ being a straight line. Otherwise $\partial U/\partial s(\mathbf{r}) = \partial U/\partial s^{\sigma t} \cdot \omega$, with $\omega = 1 + (\Delta s/\rho)$, a correction for the curvature of $\sigma^t(\mathbf{s})$ depending on the radius of curvature ρ, and the displacement of the system from the lowest free energy path $\Delta s = |\mathscr{P}\mathbf{s}(\mathbf{r}) - s^{\sigma t}|$. The operator $\mathscr{P}$ projects $\mathbf{s}(\mathbf{r})$ onto the plane of curvature for s dimensions higher than 2 (as illustrated in Figure 13). For a s dimension equal to 2, $\mathscr{P} = 1$ for $\mathbf{s}(\mathbf{r})$ located on the inner side of the curved path and $\mathscr{P} = -1$ for $s(\mathbf{r})$ located on the outer side.

References and Notes

(1) Fukui, K. *J. Am. Chem. Soc.* **1970**, *74*, 4160.
(2) Fukui, K. *Acc. Chem. Res.* **1981**, *14*, 363.

Computations for Concerted Reactions

J. Phys. Chem. B, Vol. 109, No. 14, 2005 **6687**

(3) Scientific Computing & Modeling. *ADF 2002.01*, Theoretical Chemistry, Vrije Universiteit: Amsterdam, The Netherlands, 2002 (http://www.scm.com).

(4) *CPMD*, version 3.5; IBM Corp., MPI fuer Festkoerperforschung Stuttgard: Stuttgart, 2001.

(5) Frisch, M. J.; Trucks, G. W.; Schlegel, H. B.; Scuseria, G. E.; Robb, M. A.; Cheeseman, J. R.; Zakrzewski, V. G.; Montgomery, J. A., Jr.; Stratmann, R. E.; Burant, J. C.; Dapprich, S.; Millam, J. M.; Daniels, A. D.; Kudin, K. N.; Strain, M. C.; Farkas, O.; Tomasi, J.; Barone, V.; Cossi, M.; Cammi, R.; Mennucci, B.; Pomelli, C.; Adamo, C.; Clifford, S.; Ochterski, J.; Petersson, G. A.; Ayala, P. Y.; Cui, Q.; Morokuma, K.; Malick, D. K.; Rabuck, A. D.; Raghavachari, K.; Foresman, J. B.; Cioslowski, J.; Ortiz, J. V.; Stefanov, B. B.; Liu, G.; Liashenko, A.; Piskorz, P.; Komaromi, I.; Gomperts, R.; Martin, R. L.; Fox, D. J.; Keith, T.; Al-Laham, M. A.; Peng, C. Y.; Nanayakkara, A.; Gonzalez, C.; Challacombe, M.; Gill, P. M. W.; Johnson, B. G.; Chen, W.; Wong, M. W.; Andres, J. L.; Head-Gordon, M.; Replogle, E. S.; Pople, J. A. *Gaussian 98*; Gaussian, Inc.: Pittsburgh, PA, 1998.

(6) Cerjan, C. J.; Miller, W. H. *J. Chem. Phys.* **1981**, *75*, 2800.

(7) Baker, J. *J. Comput. Chem.* **1988**, *9*, 465.

(8) Henkelman, G.; Jónsson, H. *J. Chem. Phys.* **1999**, *111*, 7010.

(9) Peters, B.; Liang, W.; Bell, A. T. *J. Chem. Phys.* **2003**, *118*, 9533.

(10) Ayala, P. Y.; Schlegel, H. B. *J. Chem. Phys.* **1997**, *107*, 375.

(11) Voter, A. F. *J. Chem. Phys.* **1996**, *106*, 4665.

(12) Pratt, L. R. *J. Chem. Phys.* **1986**, *85*, 5045.

(13) Dellago, C.; Bolhuis, P. G.; Csajka, F. S.; Chandler, D. *J. Chem. Phys.* **1998**, *108*, 1964.

(14) Passerone, D.; Parrinello, M. *Phys. Rev. Lett.* **2001**, *87*, 108302.

(15) Hummer, G.; Kevrekidis, I. G. *J. Chem. Phys.* **2003**, *118*, 10762.

(16) Park, S.; Sener, M. K.; Lu, D.; Schulten, K. *J. Chem. Phys.* **2003**, *119*, 1313.

(17) Henkelman, G.; Jónsson, H. *J. Chem. Phys.* **2000**, *113*, 9978.

(18) Weinan, E.; Ren, W.; Vanden-Eijnden, E. *Phys. Rev. B* **2002**, *66*, 052301.

(19) den Otter, W. K.; Briels, W. J. *J. Chem. Phys.* **1997**, *106*, 5494.

(20) Geissler, P. L.; Dellago, C.; Chandler, D. *J. Phys. Chem. B* **1999**, *103*, 3706.

(21) Ensing, B.; Meijer, E. J.; Blöchl, P. E.; Baerends, E. J. *J. Phys. Chem. A* **2001**, *105*, 3300.

(22) Blumberger, J.; Sprik, M. *J. Phys. Chem. B* **2004**, *108*, 6529.

(23) Geissler, P. L.; Chandler, D. *J. Chem. Phys.* **2000**, *113*, 9759.

(24) Laio, A.; Parrinello, M. *Proc. Natl Acad. Sci. U.S.A.* **2002**, *99*, 12562.

(25) Iannuzzi, M.; Laio, A.; Parrinello, M. *Phys. Rev. Lett.* **2003**, *90*, 238302.

(26) Huber, T.; Torda, A. E.; van Gunsteren, W. F. *J. Comput.-Aided Mol. Des.* **1994**, *8*, 695.

(27) Ensing, B.; Laio, A.; Gervasio, F. L.; Parrinello, M.; Klein, M. L. *J. Am. Chem. Soc.* **2004**, *126*, 9492.

(28) Car, R.; Parrinello, M. *Phys. Rev. Lett.* **1985**, *55*, 2471.

(29) Press, W. H.; Vetterling, W. T. *Numerical Recipes in FORTRAN 90*, 2nd ed.; Cambridge University Press: Cambridge, 1996.

(30) Marx, D.; Hutter, J. Ab Initio Molecular Dynamics: Theory and Implementation. In *Modern Methods and Algorithms of Quantum Chemistry*; Grotendorst, J., Ed.; NIC Series; John von Neumann Institute for Computing: Jólich, Germany, 2000; p 301.

(31) Becke, A. D. *Phys. Rev. A* **1988**, *38*, 3098.

(32) Lee, C.; Yand, W.; Parr, R. G. *Phys. Rev. B* **1988**, *37*, 785.

(33) Troellier, N.; Martins, J. L. *Phys. Rev. B* **1991**, *43*, 1993.

(34) Martyna, G. J.; Tuckerman, M. E. *J. Chem. Phys.* **1999**, *110*, 2810.

(35) Gritsenko, O. V.; Ensing, B.; Schipper, P. R. T.; Baerends, E. J. *J. Phys. Chem. A* **2000**, *104*, 8558.

(36) Kumar, S.; Bouzida, D.; Swendsen, R. H.; Kollman, P. A.; Rosenberg, J. M. *J. Comput. Chem.* **1992**, *13*, 1011.